The evolution of aerosols mixing state derived from a field campaign in Beijing: implications to the particles aging time scale in urban atmosphere

Jieyao Liu[1], Fang Zhang[2], Jingye Ren[3], Lu Chen[4], Anran Zhang[2], Zhe Wang[2], Songjian Zou[2], Honghao Xu[2], Xingyan Yue[1]

[1] School of Geographical Sciences, Hebei Normal University, Shijiazhuang, China

[2] School of Civil and Environmental Engineering, Harbin Institute of Technology (Shenzhen), Shenzhen, China

[3] Xi'an Institute for Innovative Earth Environment Research, Xi'an, China

[4] Faculty of Geographical Science, Beijing Normal University, Beijing, China

Correspondence to: Fang Zhang (zhangfang2021@hit.edu.cn)

Abstract

The mixing states and aging time scale of aerosol particles play a vital role in evaluating their climate effects. Here, by using the field measurement at a site of the urban Beijing, we have identified four different real-time mixing patterns of size-resolved particles, which are defined as less hygroscopic (LH) internally-mixed, externally-mixed, transitional externally-mixed and more hygroscopic (MH) internally-mixed particles, with atmospheric fraction of 0-10%, 20-46%, 17-24% and 27-56% respectively. The fraction depends on particles size, with the maximum fraction of MH internally-mixed particles at 80 and 110 nm, and the minimum fraction of LH internally-mixed particles across all sizes, implying rapid mixing and aging of ambient particles during the observational period. The diurnal variations of the mixing states of particles in all sizes investigated (40, 80, 110, 150 and 200 nm) present an apparent aging process from externally-mixed to MH internally-mixed, which typically spans

26 a duration of approximately 5–10 hours from 8:00–10:00 to 15:00–17:00, revealing the

27 mixing (aging) timescale of aerosols in polluted urban atmosphere. Additionally, our results

28 suggest that those fine aerosol particles experience aging through both the photochemical

29 process and non-photochemical growth during the campaign. Furthermore, through a

30 comprehensive review of the mixing/aging timescale of particles adopted in current models

31 and derived from observations, we show the great discrepancy between observations and

32 models, highlighting the importance to parameterize their aging time scale based on more

33 field campaigns.

34

35 **1 Introduction**

36   The mixing state of atmospheric aerosol particles can affect the hygroscopicity and the

37 ability to serve as cloud condensation nuclei (CCN), and thus the air quality and climate

38 (Müller et al., 2017; Xu et al., 2021; Yao et al., 2022; Ge et al., 2024). It has been shown that

39 the aerosol mixing state is closely related to the hygroscopicity (Chen et al., 2022; Fan et al.,

40 2020). Ren et al. (2018) predicted the concentration of CCN using five different mixing state

41 schemes and found that the influence of aerosol mixing state on its activation characteristics

42 ranged from –34% to +16%. Neglecting particle mixing structure can also lead to significant

43 overestimation of the aerosol absorption efficiency (Yao et al., 2022). Therefore, it is

44 important to account for the information of mixing state of ambient particles in climate

45 models so as to reduce the uncertainty in evaluating their environmental and climate effects.

46   The mixing states of ambient particles are complex. Particles in areas affected by

47 primary emissions are mainly with external mixing state (i.e., the chemical components of

48 particles exist independently), while aerosols in relatively clean areas are mainly transported

49 from elsewhere and have a higher degree of internal mixing (Swietlicki et al., 2008; Enroth et

50 al., 2018; Chen et al., 2022). Internal mixing typically includes uniform composition or core–

51 shell structures (Jacobson et al., 2001). The former refers to the same proportion of species in

52 any part of the aerosol component, while the latter is defined as the mixing state formed by

53 certain chemical components coating or condensing on the surface of other components

54 during the aging process. Also, the mixing state of aerosol particles is variable. Freshly

55 emitted particles undergo various processes, including photochemical and aqueous-phase

56 processes, as well as physical processes such as coagulation and condensation, leading to an

57 increase in their degree of internal mixing. This gradual transition from external to internal

58 mixing characterizes the aging process of particles. The aging timescale varies greatly

59 between clean and polluted areas (Peng et al., 2016; Chen et al., 2017; Ghosh et al., 2021).

60 However, the timescale of aging process of particles was commonly fixed in many models

61 and did not depend on environmental conditions (Chen et al., 2017; Ghosh et al., 2021),

62 which may introduce great uncertainty in the prediction of regional aerosol concentration and

63 the evaluation of aerosol climate effects (Ghosh et al., 2021). Therefore, capturing the

64 temporal scales of the evolution of the aerosol mixing state based on field campaigns is

65 crucial for accurately parameterizing the aging timescale of aerosol particles in models,

66 thereby enhancing the precision of simulations pertaining to the environmental and climatic

67 impacts of aerosols.

68   At present, some studies have characterized the mixing state and aging process of black

69 carbon (BC) aerosols using different instruments. Transmission electron microscopy (TEM)

70 has been used to determine the mixing state of individual particles in China (Li et al., 2016;

71 Zhang et al., 2023). However, based on TEM technique, a large number of aerosol samples

72 are required so as to make the results with the significance of statistics, which means a high

73 cost both on labors and materials. The most important issue is that the mixing state of

74 particles may change during collection and transportation. Recently, aerosol time-of-flight

75 mass spectrometry (ATOFMAS) and soot-particle aerosol mass spectrometry (SP-AMS) have

76 been used to measure the mixing state of BC and coated aerosol species in real time (Liu et

77 al., 2019; Xie et al., 2020). Overall, previous studies focused more on the mixing state of BC

78 of single-particles (Saha et al., 2018; Xie et al., 2020; Chen et al., 2020). While, the mixing

79 state of particles across a population in ambient atmosphere is more complex (Riemer et al.,

80 2019). According to Winkler's definition, the "internal mixing" means when all particles

81 within the bulk aerosol populations are with the same compositions. While, the "external

82 mixing" means when all particles consist of pure species and have distinct compositions

83 (Winkler et al., 1973; Riemer et al., 2019). Note that in Riemer et al. (2019), the definition

84 refers to the bulk not the sized-resolved mixing state of aerosol particles. In this study, the

85 size resolved mixing state of aerosol particles has been identified according to the patterns of

86 the probability density function of hygroscopic growth factor/hygroscopic parameter (κ) (Gf-

87 PDF; κ-PDF) measured using a humidity tandem differential mobility analyzer (H-TDMA)

88 (Hong et al., 2018; Shi et al., 2022; Spitieri et al., 2023). For example, the internally-mixed

89 aerosol populations with diameter of 40 nm are characterized by the single hygroscopic mode

90 of Gf-PDF/κ-PDF, while the externally-mixed particles have bi- or trimodal distributions of

91 Gf-PDF/κ-PDF. However, most studies based on the H-TDMA measurements only made

92 qualitative descriptions of the particle mixing state when explaining the variations in the

93 aerosol hygroscopicity (Wang et al., 2019; Chen et al., 2022; Shi et al., 2022).

94   In this study, with the aim of obtaining insights into the mixing state and mixing (aging)

95 time scale of ambient particles in urban area, we have identified four different types of size-

96 resolved particles mixing states, and characterized their real-time variations using the field

97 measured hygroscopic growth factor by the H-TDMA in urban Beijing. The evolution of

98 mixing state of particles with specific sizes was explored to imply the mixing (aging)

99 timescale of their aging from the diurnal variations during clear and cloudy days. Finally, we

100 compared the mixing/aging timescale of aerosol particles with that adopted in current models

101 and other field observations reported in previous literatures.

102 **2 Methods**

103   The campaign was conducted at the meteorological tower branch of the Institute of

104 Atmospheric Physics (IAP), Chinese Academy of Sciences to measure the physical and

105 chemical properties of particles and the meteorological conditions from 19 May to 18 June

106 2017 in Beijing. The instruments used in this study were deployed in a container at ground

107 (the sampling inlet is located at ∼8 m on the meteorological tower). The hygroscopicity of

108 aerosols with different dry sizes (40, 80, 110, 150 and 200 nm) and particle number

109 distribution in the size range of 10–550 nm was measured using a H-TDMA and a Scanning

110 Mobility Particle Sizer (SMPS), respectively. The mass concentration of the non-refractory

111 chemical compositions in particulate matter with diameter < 1 μm (PM_1) was measured by an

112 Aerodyne high-resolution time-of-flight aerosol mass spectrometer (HR-ToF-AMS) (Xu et al.,

113 2019), and the BC was measured by a 7-wavelength aethalometer (AE33, Magee Scientific

114 Corp). More details about the sites, instruments and calibrations can be found in previous

115 literatures (Zhang et al., 2017; Wang et al., 2019; Fan et al., 2020; Chen et al., 2022). Since

116 the campaign site was located at the urban area of Beijing, where the atmospheric fine

117 aerosols are more frequently affected by local traffic and cooking sources (Sun et al., 2015).

118   In addition, during the observation period of summertime, the site was predominately

119   affected by the warm and humid southeastern air parcels (Figure S1); while the dust events

120   normally originate from northwestern regions occurring in springtime (Li et al., 2020) and

121   typically with particle sizes in coarse mode (Wang et al., 2023). Therefore, the contribution

122   from dust aerosols could be negligible in this study.

123   Here, we mainly describe the interpretation criteria for the mixing state of particles. The

124   Gf-PDF was obtained by TDMA$_{inv}$ algorithm in this study (Gysel et al., 2009). Then, the κ-

125   PDF of size-resolved particles was retrieved according to the κ-Köhler theory (Petters and

126   Kreidenweis, 2007). Subsequently, we accurately defined four mixing states based on the

127   κ-PDF patterns and the number of peaks in κ-PDF (Figure 1, Figure S2). The κ-PDF of type 1

128   exhibits bimodal distributions with a much higher proportion (> 70%) of hydrophobic mode

129   or less hygroscopic mode (LH; the peak of κ-PDF occurs at $\kappa < 0.1$), was thus defined as LH

130   internally-mixed state (type 1). Mixing type 2 refers to that the κ-PDF exhibits bimodal

131   distributions in both LH and more hygroscopic (MH, $\kappa \geq 0.1$) modes, with the difference of

132   less than 30% between the fraction of the two modes. The κ-PDF pattern with trimodal

133   distributions was named as transitional externally-mixed state (type 3). The κ-PDF of type 4

134   was dominated by MH mode, normally with a fraction of lager than 70%, was defined as MH

135   internally-mixed type. It should be noted that the four categories defined in our study have

136   covered all cases of the observational results. In this study, we also calculated the standard

137   deviation of κ-PDF (σ) according to Spitieri et al. (2023), which indicates the degree of

138   dispersion in the data, and is thought to reflect the mixing degree of particles to a certain

139   extent. Given that the aerosol particles sampled at the campaign site in this study are rarely

140   affected by other hygroscopic aerosols (e.g., aerosols from marine sources), the MH

141   internally-mixed particles (110, 150 and 200 nm) are thus mainly from the aging and growth

142   of smaller particles. In contrast, the larger LH internally-mixed particles are predominantly

143 from primary emissions. Therefore, the proportion of MH and LH internally-mixed particles

144 at 100-200 nm can be used to distinguish the contribution to the internally-mixed fraction of

145 larger particles from smaller aerosol aging and primary emissions respectively. Specifically,

146 the result shows that a significant proportion of the internally-mixed particles at larger size

147 originate from the aging and growth of smaller particles, accounting for 99%, 96% and 92%

148 respectively for 110, 150 and 200 nm particles, whereas the contribution from primary

149 emissions to these larger internally-mixed particles is less than 10%.

150
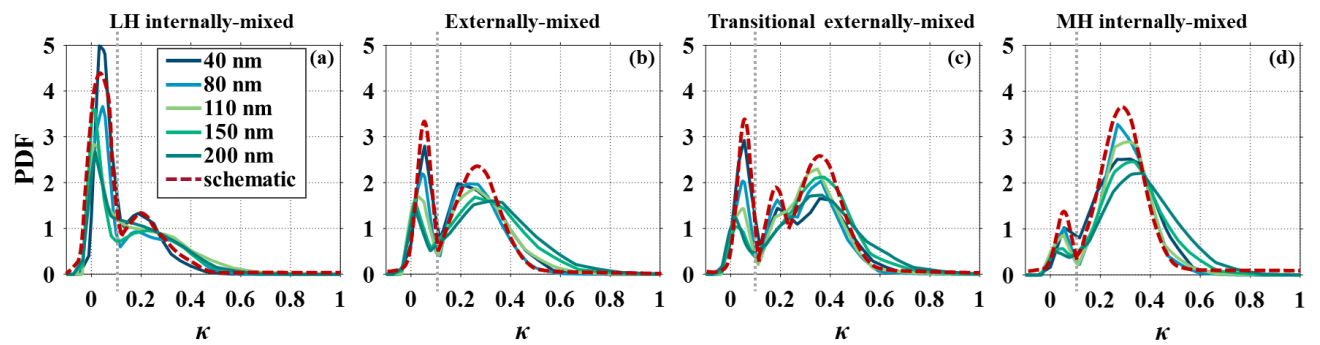
151 Figure 1. The mean κ-PDF of five particle sizes and the schematic diagram of κ-PDF for four

152 mixing types.

153 **3 Results and discussion**

154 **3.1 Overview of the mixing state of size-resolved particles**

155   Figure 2 shows the time series of size-resolved κ, and κ versus σ. The real-time changes

156 in the mixing states of particles are represented by different filled colors. The κ values vary

157 from 0 to 0.5 in each of the five particle sizes, accompanied by significant changes in mixing

158 states. In general, the mixing state of particles gradually transitions from externally-mixed to

159 MH internally-mixed along with increases in κ. For example, particles with size of 40 nm are

160 dominated by LH internally-mixed and externally-mixed at $\kappa < 0.2$; and the transitional

161 externally-mixed state take up an increasingly proportion often corresponding to κ values of >

162 0.2 and the MH internally-mixed particles occur when κ greater than 0.3 (shown by the light

163 gray dots in Figure 2).

However, there exists different correlations between κ and σ for the five sizes. For particles with diameter of 40 and 80 nm, the σ increases as the κ increases from 0.1 to 0.4 along with slight increase in the fraction of MH internally-mixed particles, showing a positive correlation. While, unlike the small particles, the σ for particles larger than 100 nm (i.e., 110, 150 and 200 nm) exhibits a negative correlation to κ variations, showing that the particles were more MH internally-mixed and with stronger hygroscopicity when the smaller σ values were derived. The different sources and chemical compositions of aerosol particles could explain the distinct relationship between σ, mixing states and hygroscopicity among particles of different sizes. Here, the standard deviation of κ-PDF, σ, reflects the degree of dispersion in the pattern of κ-PDF. Taking 40 nm particles as an example, the obtained larger σ value indicates more diversity in particles hygroscopicity and chemical compositions, and thus a higher degree of external mixing state. This is because that, besides the local emissions (Ren et al., 2023), the 40 nm particles during the campaign were also from the growth of newly formed particles which are much more hygroscopic (Liu et al., 2021a). Therefore, the composition of those small particles is more heterogeneous, resulting in both greater σ and κ. The cases where both the σ and κ of small particles are lower suggest that the particles may consist of a mixture of different species originating from primary emissions (e.g., BC, hydrocarbon-like and/or cooking organic aerosols). While, for most of larger particles, their chemical composition tends to become homogeneous after aging and growth processes, exhibiting stronger hygroscopicity, a higher degree of internal mixing, and thus the smaller σ. However, a small number of larger particles with weak hygroscopic properties from primary emissions coexist with the aged ones in the atmosphere, which would result in larger σ and higher degree of external mixing.

187
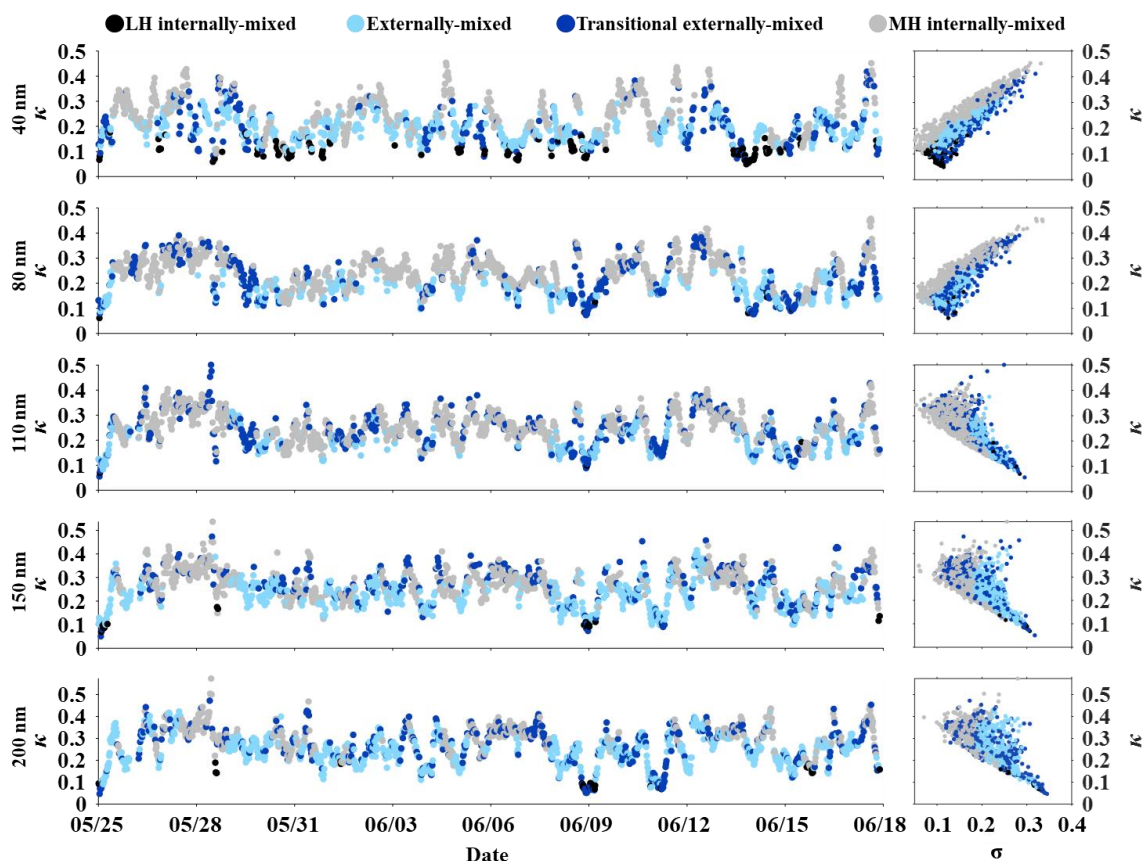
Figure 2. Time series of hygroscopic parameter (κ), and plots of κ versus standard deviation

of κ-PDF (σ) for 40, 80, 110, 150 and 200 nm particles (from top to bottom). The colors

denote the different mixing types.

The size dependence of mixing type fractions and σ are shown in Figure 3. The external

mixing types, including externally-mixed and transitional externally-mixed states, dominate

in 40, 150 and 200 nm particles, accounting for 53%, 57% and 70% respectively of all

mixing types. The elevated fraction of externally-mixed particles is intimately associated with

the local sources. For instance, a previous study revealed the particle size distribution of

aerosols from different sources in urban Beijing, suggesting that the particles with diameter

of 40 nm during rush hours and cooking times predominantly originated from primary

emissions, and particles at 150 and 200 nm displayed a strong correlation with regional

199   atmospheric transport sources (Ren et al., 2023). In this study, the particles exhibit weaker

200   hygroscopicity at lower wind speeds, indicating that hydrophobic particles are primarily from

201   local sources (Figure S3). Furthermore, for 40 nm particles, the relatively higher fraction of

202   MH internally-mixed particles (37%) is likely due to the growth and aging of newly formed

203   particles (Liu et al., 2021a). This is similar to the result observed in Athens, Greece, in which

204   the particles with 30 nm were more internally-mixed (Spitieri et al., 2023). While, for

205   particles with sizes of 80 and 110 nm, the transitional externally-mixed and MH internally-

206   mixed states totally account for 50-80% of all mixing types, corresponding to a significant

207   decrease from about 10% to less than 1% of the fraction of the LH internally-mixed type.

208   Note that the proportion of transitional externally-mixed particles remain relative constant,

209   with a mean value of 21% across all sizes in this study, implying a continuous influence of

210   atmospheric aging process on the particles mixing state. In addition, the 80 and 110 nm

211   aerosols may continue aging and form 150 and 200 nm aerosol particles. Therefore, the aging

212   of this group of aerosols should be more advanced, showing that the fraction of internally-

213   mixed particles at 80 and 110 nm was the highest among the five particle sizes. On average,

214   the result reveals that the externally and internally mixed particles accounted for 53%±11%

215   and 47%±11% respectively. The mixing state of particles derived in this study differs from

216   that reported by Zhang et al. (2017), in which they conducted the measurements at a suburban

217   site of Xinzhou, where the aerosols are much less affected by sources nearby, and the aerosols

218   are mainly transported from elsewhere and are thus more aged and well mixed. The result

219   implies that the influence of mixing state on hygroscopicity should be explored at specific

220   particle sizes due to the heterogeneity of chemical compositions with particle size (Fan et al.,

221   2020, Figure S4).

222
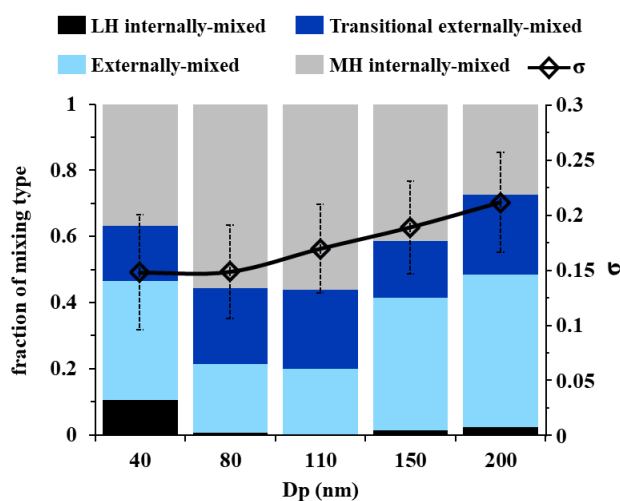
223   Figure 3. The size dependence of fraction of particles mixing types and σ.

224   Further, we compared the dependence of κ and σ on the variations of mixing states for

225   five particle sizes (Figure 4). At 40 and 80 nm sizes, it shows that both κ and σ increases

226   markedly when the particles change from externally-mixed to MH internally-mixed. While,

227   for particles with sizes of 110, 150 and 200 nm, the σ reduced but the κ increased when the

228   particles change from externally to internally-mixed state. In other words, the σ of the

229   particles larger than 80 nm shifts to lower values as the particles become more internally

230   mixed. This contrasts with that previously observed in a vegetated site by Spitieri et al.

231   (2023), which used only σ of Gf-PDF as a single indicator to characterize the particles mixing

232   state. The distinct relationship between mixing type and σ for small particles (i.e., 40 and 80

233   nm) in urban sites indicates that the standard deviation of κ-PDF can effectively characterize

234   mixing degree and chemical composition heterogeneity of larger particles in polluted area,

235   where smaller aerosol particles are usually severely affected by local anthropogenic

236   emissions.

237
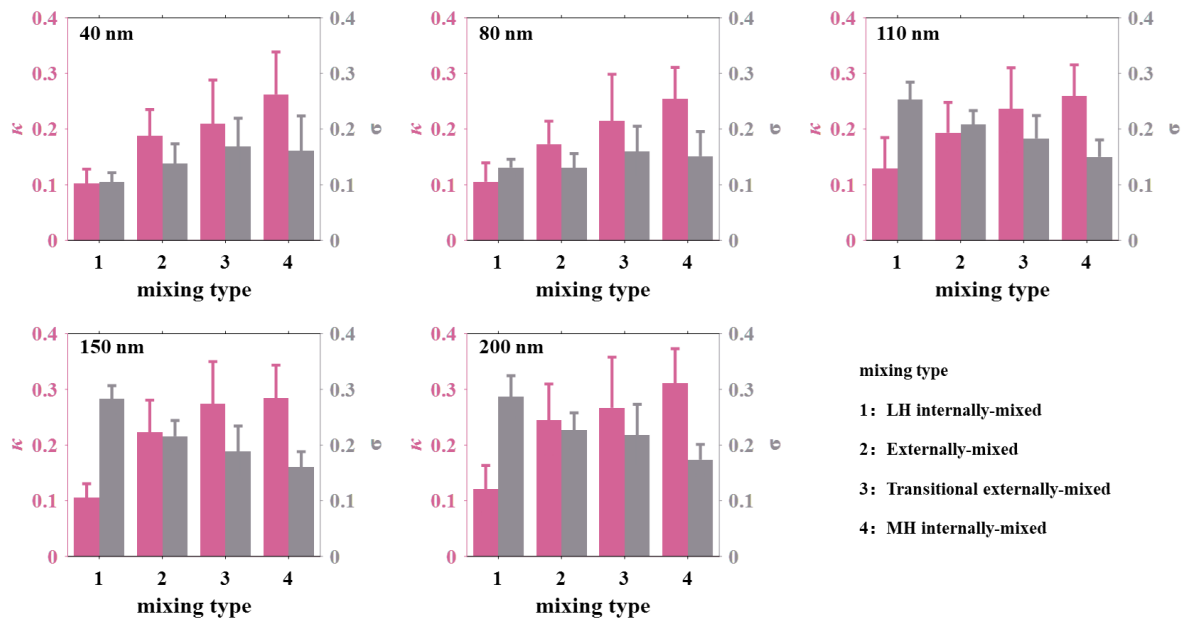
Figure 4. The mixing type dependence of hygroscopicity and σ for five particle sizes.

3.2 Evolution of mixing state of the particles

The average diurnal variations of the mixing state and κ of different particle sizes are shown in Figure 5. For 40 nm particles, the fraction of LH internally-mixed particles presents three peaks at morning (9:00–12:00 local time; LT), evening rush hours (18:00–20:00 LT) and nighttime (0:00–03:00 LT). This is accompanied with the impacts from those primary cooking and traffic emissions (Xu et al., 2021; Liu et al., 2021b). Unlike the 40 nm particles, there is no apparent increase of externally-mixed state for the particles with sizes of 80, 110, 150, and 200 nm in the rush hours or cooking times. The results indicate that the particles emitted from local primary sources are small mainly with sizes around 40 nm during the campaign. Correspondingly, the proportion of the particles with MH internally-mixed state was smallest in the morning and nighttime, but exhibiting a rapid increase from about 9:00 until the evening rush hours (about 16:00–18:00). This is accompanied by the increase of hydrophobic modes in κ-PDFs of small particle sizes during rush and cooking hours measured in Beijing (Figure S5). Moreover, the increase of externally-mixed particles of 40 nm at nighttime may be highly associated with the emissions of primary species from heavy

254 trucks in urban Beijing at nighttime (Hua et al., 2018), which can also be evidenced by the

255 increased hydrophobic mode of the 150 nm and 200 nm particles observed from 00:00 to

256 around 3:00 in Figure S5. In addition, the absence of photochemical aging and the lower

257 boundary layer height during nighttime could also result in a higher proportion of externally-

258 mixed particles. In addition, the externally-mixed and transitional externally-mixed particles

259 represent the intermediate state of the aging process in which particles transition from LH to

260 MH mode, and both showed a decrease to around 10% during the corresponding period of the

261 day as the proportion of particles with MH internally-mixed state increased up to 80%. As a

262 result, an obvious enhancement in particles hygroscopicity was observed during the daytime,

263 indicating the impact of particles mixing and aging on their hygroscopicity (Hersey et al.,

264 2013; Müller et al., 2017). Overall, the diurnal variation implies an apparent aging process

265 that leads the particles changed from externally-mixed in the early morning to MH internally-

266 mixed in the afternoon.

267
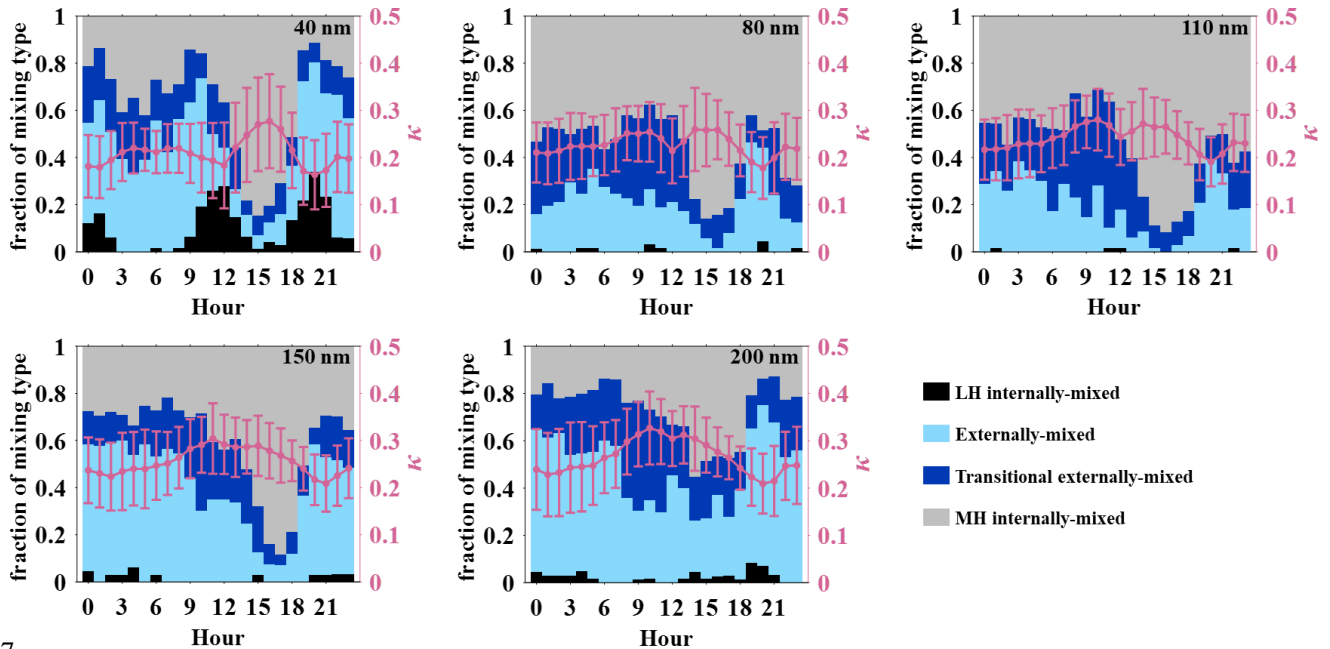
268 Figure 5. Diurnal variations of the mixing state fraction and κ for five particle sizes.

269 **3.3 Particles mixing (aging) timescale: on clear and cloudy days**

270   The aerosol particles mixing and aging process is usually accompanied by the growth of

271   particle sizes. In order to derive the mixing and aging timescale of particles, we further

272   analyzed the averaged diurnal variations of particles fraction with MH internally-mixed state,

273   particle number size distributions (PNSD) and the variations of mean κ-PDF during the

274   growth periods on both clear and cloudy days (Figure 6). On clear days, the fraction of MH

275   internally-mixed particles increases significantly from ~10-40% before 9:00 to nearly 100%

276   during 12:00–15:00, especially for particles larger than 40 nm. Such enhancement is nearly as

277   large as that on cloudy days. In detail, the proportion of MH internally-mixed particles

278   usually increased by less than 50% between the period before 9:00 and during 12:00–17:00,

279   and its maximum fraction was around 50%-90%. While, the fraction of MH internally-mixed

280   particles for 40 nm is noticeably higher on clear days (80%), which is approximately 40%

281   greater than that on cloudy days, indicating that photochemical processes can make particles

282   more internally-mixed and aged (Liu et al., 2021a). Furthermore, the diurnal variations of

283   PNSD show that the growth of particle size is highly consistent with the increase of the

284   fraction of MH internally-mixed particles. Additionally, the particles κ with large sizes at the

285   corresponding times in the PNSD also shows an increase on both clear and cloudy days.

286   Specifically, as the particle size grows from less than 40 nm before 9:00 to ~100 nm around

287   17:00, the fraction of MH internally-mixed particles increases from less than 40% to >90%.

288   And, the peak value for κ shifts from $\kappa < 0.1$ to $\kappa > 0.2$, and the count for the peak value of

289   κ-PDF increases accordingly (Figure 6). Overall, on clear days, the particles undergo a

290   gradual shift from externally-mixed to MH internally-mixed states during 8:00–16:00

291   accompanied by a growth in particle size from 20 nm to about 100 nm, which is generally 1–

292   2 hours shorter than that observed on cloudy days.

293   The obvious banana-shape growth of newly formed particles was captured in the diurnal

294   variations of PNSD, which characterizes that the aging and growth of non-hygroscopic

295   particles (e.g., BC) of primary emission and newly generated particles. Overall, the mixing

296   and aging process is confirmed by the transition of particle from externally-mixed to MH

297   internally-mixed, as well as the growth of particle size, which typically spans a duration of

298   approximately 5 to 10 hours, as is similar to the aging timescale of aerosol particles in the

299   polluted Indo-Gangetic Plain (< 10 hours) (Ghosh et al., 2021). Actually, the aerosol particles

300   aging would be largely affected by local atmospheric conditions, and thus would vary both

301   spatially and temporally (Pöschl et al., 2001; Huang et al., 2013). For example, using an

302   environmental chamber approach, Peng et al. (2016) revealed that the timescale of BC

303   aerosols aging is 2.3 and 4.6 hours, 9 and 18 hours over two cities—Beijing and Houston

304   respectively. Note that the faster aging time in Beijing derived in the chamber experiment is

305   probably due to the different levels in the concentration of gaseous precursors. In addition,

306   there is only photochemical aging occurred in the chamber experiment, however, in the

307   atmosphere, the particles aging is also through coagulation process which usually occurs

308   slower than the photochemical reaction and condensation processes (Chen et al., 2017). This

309   can also explain our observed faster mixing (aging) time on clear days when the

310   photochemical process is more significant considering that the difference of the pollutant

311   concentrations in daytime between clear and cloudy days is not obvious (i.e., O_x and PM_1;

312   Figure S6).
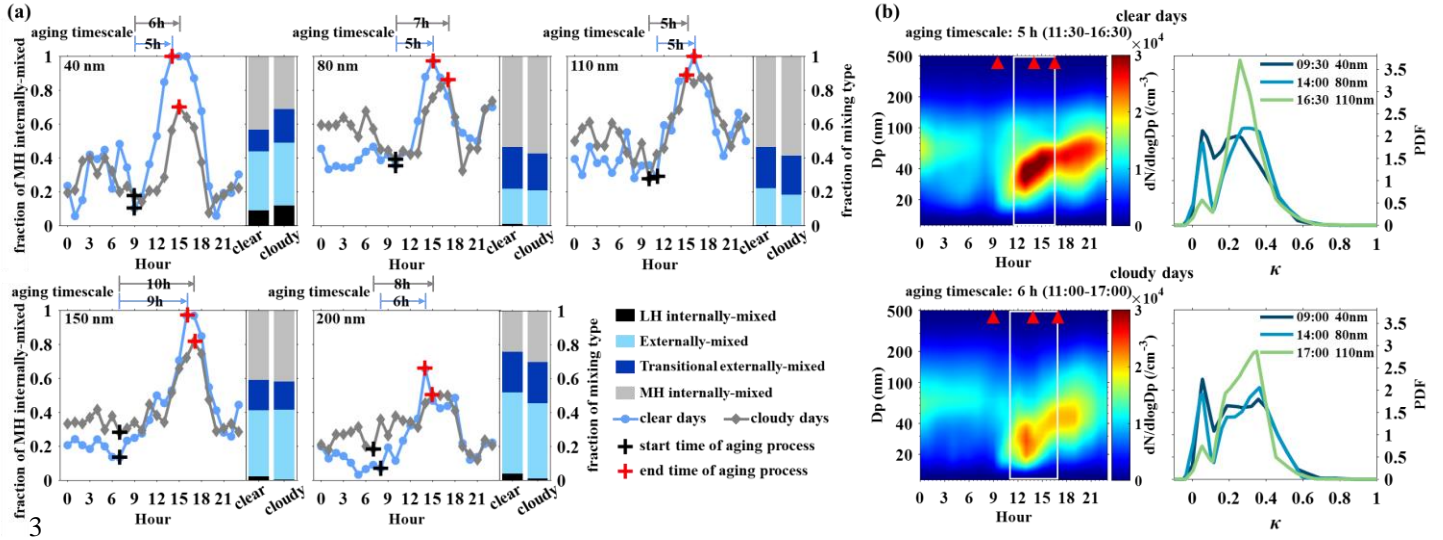
Figure 6. (a) Diurnal variations of the proportion of MH internally-mixed particles and statistical results of the fraction of mixing state for five particle sizes on clear and cloudy days. The start time of particle mixing/aging was selected when the proportion of MH internally-mixed particles is minimum between sunrise and noon, and the end time was defined as when the fraction of MH internally-mixed particles reaches its maximum. (b) The averaged diurnal variations in PNSD and the variations of mean κ-PDF during the growth periods on clear and cloudy days (right panels). The red triangles indicate 2 hours before the start of the aging, during the growth and end of the aging process respectively.

3.4 Implications to parameterization of the current models

The mixing/aging timescale of aerosol particles significantly impacts their physiochemical properties, which in turn affects their atmospheric lifetime, transport characteristics (Zhang et al., 2023), hygroscopicity and the direct radiative forcing of aerosol particles (Moffet and Prather, 2009; Wang et al., 2018; Stevens and Dastoor, 2019). We further compared our results with the results derived from five field sites and the values adopted in current models (Table S1). In most models, the aging processes of carbonaceous aerosols were treated with a simple parameterization, which generally obtained aging time based on the transformation of aerosols from hydrophobic to hydrophilic (Chen et al., 2017;

331 Ghosh et al., 2021). Unlike the models, the aging timescale of BC aerosols in field

332 measurements and laboratory studies was commonly derived by tracking changes in

333 hygroscopicity, morphology, coating thickness or optical properties (Moffet and Prather, 2009;

334 Akagi et al., 2012; Krasowsky et al., 2016; Peng et al., 2016). These methods were used to

335 quantify the aging timescale of particles indirectly. While, in our study, the mixing (aging)

336 time was inferred based on the changes in hygroscopic modes and mixing states of non-BC

337 particles in the ambient atmosphere. Note that although there may be some differences in the

338 results based on different methods, the aging timescales obtained all represent the mixing and

339 aging rate of aerosol particles in the atmosphere, which affects aerosols atmospheric lifetime,

340 thus the environment and climate effects. As shown in Figure 7, the derived aging timescale

341 of aerosols in this study is comparable to the observational results reported in other urban

342 areas, such as Mexico City (3 hours; Moffet and Prather, 2009) and Los Angeles (3 hours;

343 Krasowsky et al., 2016). The result is also close to the aging timescale of particles in source

344 area of biomass burning in California (4 hours; Akagi et al., 2012). However, the aging time

345 of particles displays large spatial variations at different sites. For example, the aging

346 timescale of particles observed in Beijing (4.6 hours) was four times faster than that in

347 Houston (18 hours) where the precursors concentrations are extremely low (Peng et al., 2016).

348 Overall, the mixing/aging timescale of particles in Beijing achieved in this study is 5–10

349 hours, which falls within the range of 2–10 hours in polluted areas obtained by other studies.

350 Therefore, our results are likely representative of the aging time scale of aerosols in polluted

351 urban areas. Furthermore, the aging time of particles obtained in ambient atmosphere is much

352 shorter than the default values adopted in most models, which is commonly with a duration of

353 1.15–2.5 days. In addition, the values among different models range greatly from 1 to 20 days

354 (Figure 7). For example, a timescale of 20 days was used to represent a slow aging process

355 (i.e., coagulation) by Liu et al. (2011), as may be not properly applied in regions with high

356   particle number concentration where the particles coagulation is also efficient (Chen et al.,

357   2017).

358   Although using a dynamic parameterization scheme for particles aging in models could

359   achieve the application of different aging times to different regions, the simulated values

360   show large variations among different models. For example, in RegCM4 model, the

361   conversion time from fresh to aged BC ranges from about 5 hours to 7 days (Ghosh et al.,

362   2021). The range in the KAMM/DRAIS, however, is only 2 hours to about 1.6 days (Riemer

363   et al., 2004). Moreover, even in central-eastern China, the aging timescale has been reported

364   to range from 12 hours to 7 days based on a regional chemical transport model (Chen et al.,

365   2017), which is much longer than that derived in urban Beijing by this study. Additionally,

366   the aging times of carbonaceous aerosols simulated by the GEOS-Chem model exhibit large

367   spatial and temporal variations, with the global average calculated to be 3.1 days (Huang et

368   al., 2013). This value is much longer than the default values used in other global models (1-2

369   days) (Pierce et al., 2007). Note that although the mixing (aging) timescale of particles was

370   determined by examining diurnal variations in the mixing state of aerosol particles in this

371   study, compared with laboratory studies, various factors in the real ambient atmosphere

372   change over time, including meteorological conditions, emission sources, and atmospheric

373   processes etc. Therefore, the result derived in this study warrants further verifications. The

374   long-term field measurements at more sites should be conducted in the future.

375   The large uncertainties in the aging timescale can significantly affect the accuracy of

376   simulation and assessment for atmospheric lifetime, loading and radiation forcing of aerosols.

377   For example, to better simulate the intercontinental transport of aerosols, Huang et al. (2013)

378 implemented a variable aging scheme in the GEOS-Chem model, which showed that the total

379 atmospheric burdens and global average lifetimes of BC (OC, organic carbon) were increase

380 by 8% (2%) compared to the default value (1.15 days). Similarly, due to the implementation

381 of the dynamic aging scheme in models, the column burden and surface mass concentration

382 of carbonaceous aerosols increased during the dry season in the polluted Indo-Gangetic Plain,

383 and the atmospheric heating increased by at least 1.2 W m^{-2} (Ghosh et al., 2021). Therefore,

384 given the large spatiotemporal variations in aging timescale of particles, the study emphasizes

385 the urgency of conducting investigations at more field sites. In addition, the other factors such

386 as the meteorology and particle sizes that affect the aerosols aging should be accounted for so

387 as to improve the dynamic aging schemes in climate models.

388
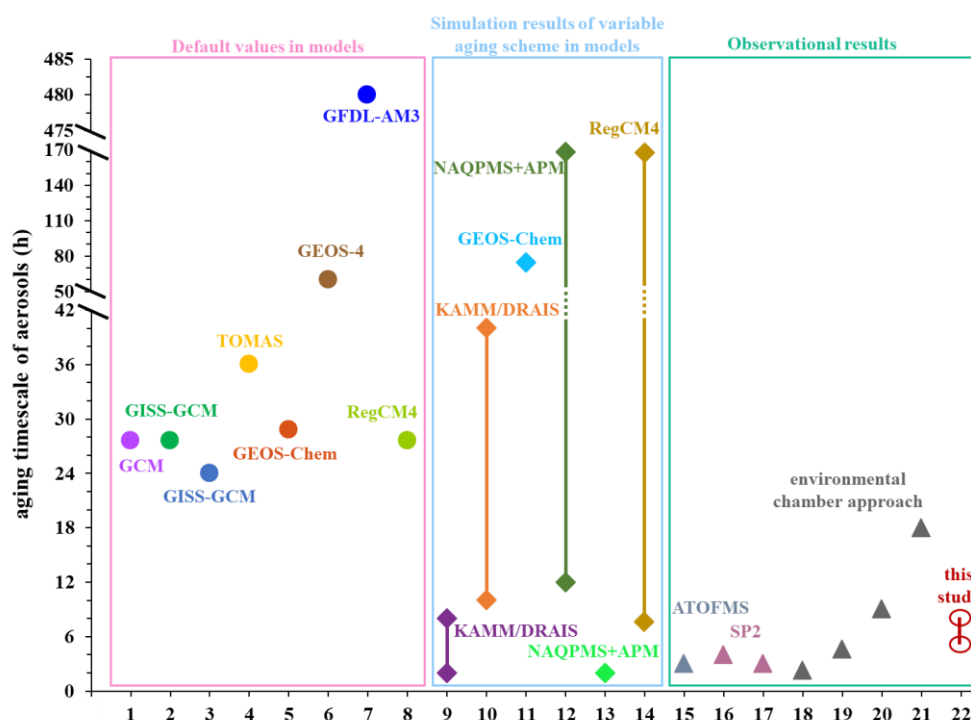
389 Figure 7. The mixing/aging timescale of particles reported in literatures (1. Cooke et al., 2002;

390 2. Chung and Seinfeld, 2002; 3. Koch and Hansen, 2005; 4. Pierce et al., 2007; 5. Yu and Luo,

391 2009; 6. Colarco et al., 2010; 7. Liu et al., 2011; 8, 14. Ghosh et al., 2021; 9, 10. Riemer et al.,

392 2004; 11. Huang et al., 2013; 12, 13. Chen et al., 2017; 15. Moffet and Prather, 2009; 16.

393 Akagi et al., 2012; 17. Krasowsky et al., 2016; 18-21. Peng et al., 2016). The solid circle,

394 diamond and the triangle denote the default aging time of particles used in models and

395 stimulation results of variable aging scheme in models, as well as the observational results,

396 respectively.

397 **4 Conclusions**

398   The real-time mixing state of ambient aerosol particles with dry particle sizes of 40, 80,

399 110, 150 and 200 nm was investigated in urban Beijing, according to PDF of hygroscopic

400 growth factor measured using the H-TDMA system. Four mixing states of ambient size-

401 resolved particles were captured in this study. In general, particles with LH internally-mixed,

402 externally-mixed, transitional externally-mixed and MH internally-mixed state account for 0-

403 10%, 20-46%, 17-24% and 27-56% respectively, which depends on particles size greatly. The

404 fraction of internally-mixed particles peaks at 80 and 110 nm due to enhanced aging in

405 intermediate particles. The diurnal variation of mixing state of particles in all sizes considered

406 presents a visible aging process, showing that the fraction of particles with MH internally-

407 mixed state increases significantly from ~10-40% before 9:00 to about 100% during 12:00–

408 15:00 on clear days, accompanied by a growth in particle size from 20 nm to 100 nm.

409 Typically, the mixing/aging process of particles takes approximately 5–10 hours, which

410 reveals the mixing (aging) timescale of aerosols during the campaign. Additionally, our

411 results suggest that fine aerosol particles undergo significant aging through photochemical

412 processes in the polluted atmosphere of urban Beijing. Furthermore, the large difference of

413 mixing/aging timescale of particles between values in models and the timescale achieved by

observations, emphasizing the vital role of exploring the aging timescale through more field measurements to improve the accuracy of aging schemes in climate models. The results revealed in our study highlight the considerable impact of atmospheric aging on mixing state of fine aerosol particles in polluted megacities.

Data availability

All data used in the study are available from the corresponding author upon request (zhangfang2021@hit.edu.cn).

Author contributions

FZ and JL conceived the conceptual development of the paper. FZ directed and performed of the experiments with JR, LC and JL. JL conducted the data analysis and wrote the draft. All authors edited and commented on the various sections of the paper.

Competing interests

The authors declare that they have no conflict of interest.

Acknowledgments

This work was funded by the National Natural Science Foundation of China (NSFC) research project (Grant No. 42475112, 42405191), Shenzhen Science and Technology Plan Project (Grant No. GXWD20220811174022002; KCXST20221021111404011), Guangdong Natural Science Foundation (Grant No. 2024A1515011005), Hebei Natural Science Foundation (Grant No. D2024205006). We thank all participants in the field campaigns for their tireless work and cooperation.

Reference

Akagi, S. K., Craven, J. S., Taylor, J. W., McMeeking, G. R., Yokelson, R. J., Burling, I. R., Urbanski, S. P., Wold, C. E., Seinfeld, J. H., Coe, H., Alvarado, M. J., and Weise, D. R.: Evolution of trace gases and particles emitted by a chaparral fire in California, Atmos. Chem. Phys., 12, 1397–1421, https://doi.org/10.5194/acp-12-1397-2012, 2012.

Chen, L., Zhang, F., Yan, P., Wang, X., Sun, L., Li, Y., Zhang, X., Sun, Y., and Li, Z.: The large proportion of black carbon (BC)-containing aerosols in the urban atmosphere, Environ. Pollut., 263, Part B, https://doi.org/10.1016/j.envpol.2020.114507, 2020.

Chen, L., Zhang, F., Zhang, D., Wang, X., Song, W., Liu, J., Ren, J., Jiang, S., Li, X., and Li, Z.: Measurement report: Hygroscopic growth of ambient fine particles measured at five sites in China, Atmos. Chem. Phys., 22, 6773–6786, https://doi.org/10.5194/acp-22-6773-2022, 2022.

Chen, X., Wang, Z., Yu, F., Pan, X., Li, J., Ge, B., Wang, Z., Hu, M., Yang, W., and Chen, H.: Estimation of atmospheric aging time of black carbon particles in the polluted atmosphere over central-eastern China using microphysical process analysis in regional chemical transport model, Atmos. Environ., 163, 44–56, https://doi.org/10.1016/j.atmosenv.2017.05.016, 2017.

Chung, S., and Seinfeld, J.: Global distribution and climate forcing of carbonaceous aerosols, J. Geophys. Res.-Atmos., 107(D19), 4407, https://doi.org/10.1029/2001JD001397, 2002.

Colarco, P., Silva, A., Chin, M., and Diehl, T.: Online simulations of global aerosol distributions in the NASA GEOS-4 model and comparisons to satellite and ground-based aerosol optical depth, J. Geophys. Res.-Atmos., 115, D14207,

https://doi.org/10.1029/2009JD012820, 2010.

Cooke, W., Ramaswamy, V., and Kasibhatla, P.: A general circulation model study of the global carbonaceous aerosol distribution, J. Geophys. Res.-Atmos., 107(D16), https://doi.org/10.1029/2001JD001274, 2002.

Enroth, J., Mikkilä, J., Németh, Z., Kulmala, M., and Salma, I.: Wintertime hygroscopicity and volatility of ambient urban aerosol particles, Atmos. Chem. Phys., 18, 4533–4548, https://doi.org/10.5194/acp-18-4533-2018, 2018.

Fan, X., Liu, J., Zhang, F., Chen, L., Collins, D., Xu, W., Jin, X., Ren, J., Wang, Y., Wu, H., Li, S., Sun, Y., and Li, Z.: Contrasting size-resolved hygroscopicity of fine particles derived by HTDMA and HR-ToF-AMS measurements between summer and winter in Beijing: the impacts of aerosol aging and local emissions, Atmos. Chem. Phys., 20, 915–929, https://doi.org/10.5194/acp-20-915-2020, 2020.

Ge, S., Su, J., Zhao, P., Li, J., Liu, S., Qiu, Y., Pu, W., and Ma, Z.: Characteristics of $PM_{2.5}$ hygroscopicity and the influences of water-soluble ions during haze events in Beijing, Atmos. Environ., 120382, https://doi.org/10.1016/j.atmosenv.2024.120382, 2024.

Ghosh, S., Riemer, N., Giuliani, G., Giorgi, F., Ganguly, D., and Dey, S.: Sensitivity of carbonaceous aerosol properties to the implementation of a dynamic aging parameterization in the regional climate model RegCM, J. Geophys. Res.-Atmos., 126, https://doi.org/10.1029/2020JD033613, 2021.

Gysel, M., McFiggans, G. B., and Coe, H.: Inversion of tandem differential mobility analyser (TDMA) measurements, J. Aerosol Sci., 40, 134–151, https://doi.org/10.1016/j.jaerosci.2008.07.013, 2009.

480 Hersey, S. P., Craven, J. S., Metcalf, A. R., Lin, J., Lathem, T., Suski, K., Cahill, J., Duong,

481   H., Sorooshian, A., Jonsson, H., Shiraiwa, M., Zuend, A., Nenes, A., Prather, K., Flagan,

482   R., and Seinfeld, J.: Composition and hygroscopicity of the los angeles aerosol: CalNex,

483   J. Geophys. Res.-Atmos., 118(7): 3016-3036, https://doi.org/10.1002/jgrd.50307, 2013.

484 Hong, J., Xu, H., Tan, H., Yin, C., Hao, L., Li, F., Cai, M., Deng, X., Wang, N., Su, H., Cheng,

485   Y., Wang, L., Petäjä, T., and Kerminen, V.-M.: Mixing state and particle hygroscopicity

486   of organic-dominated aerosols over the Pearl River Delta region in China, Atmos. Chem.

487   Phys., 18, 14079–14094, https://doi.org/10.5194/acp-18-14079-2018, 2018.

488 Hua, Y., Wang, S., Jiang, J., Zhou, W., Xu, Q., Li, X., Liu, B., Zhang, D., and Zheng, M.:

489   Characteristics and sources of aerosol pollution at a polluted rural site southwest in

490   Beijing,   China,   Sci.   Total   Environ.,   626,   519-527,

491   https://doi.org/10.1016/j.scitotenv.2018.01.047, 2018.

492 Huang, Y., Wu, S., Dubey, M. K., and French, N. H. F.: Impact of aging mechanism on model

493   simulated   carbonaceous   aerosols,   Atmos.   Chem.   Phys.,   13,   6329–6343,

494   https://doi.org/10.5194/acp-13-6329-2013, 2013.

495 Jacobson, M.: Strong radiative heating due to the mixing state of black carbon in atmospheric

496   aerosols, Nature, 409, 695–697, https://doi.org/10.1038/35055518, 2001.

497 Koch, D., Hansen, J.: Distant origins of Arctic black carbon: A Goddard Institute for Space

498   Studies   Model   experiment,   J.   Geophys.   Res.-Atmos.,   110,   D04204,

499   https://doi.org/10.1029/2004JD005296, 2005.

500 Krasowsky, T., McMeeking, G., Wang, D., Sioutas, C., Ban-Weiss, G.: Measurements of the

501   impact of atmospheric aging on physical and optical properties of ambient black carbon

particles in Los Angeles, Atmos. Environ., 142, 496-504, https://doi.org/10.1016/j.atmosenv.2016.08.010, 2016.

Liu, D., Joshi, R., Wang, J., Yu, C., Allan, J. D., Coe, H., Flynn, M. J., Xie, C., Lee, J., Squires, F., Kotthaus, S., Grimmond, S., Ge, X., Sun, Y., and Fu, P.: Contrasting physical properties of black carbon in urban Beijing between winter and summer, Atmos. Chem. Phys., 19, 6749–6769, https://doi.org/10.5194/acp-19-6749-2019, 2019.

Liu, J., Fan, S., Horowitz, L., and Levy II, H.: Evaluation of factors controlling long-range transport of black carbon to the Arctic, J. Geophys. Res.-Atmos., 116, D04307, https://doi.org/10.1029/2010JD015145, 2011.

Liu, J., Zhang, F., Xu, W., Sun, Y., Chen, L., Li, S., Ren, J., Hu, B., Wu, H., and Zhang, R.: Hygroscopicity of organic aerosols linked to formation mechanisms, Geophys. Res. Lett., 48, e2020GL091683, https://doi.org/10.1029/2020GL091683, 2021a.

Liu, J., Zhang, F., Xu, W., Chen, L., Ren, J., Jiang, S., Sun, Y., and Li, Z.: A large impact of cooking organic aerosol (COA) on particle hygroscopicity and CCN activity in urban atmosphere, J. Geophys. Res.-Atmos., 126, e2020JD033628, https://doi.org/10.1029/2020JD033628, 2021b.

Li, S., Zhang, F., Jin, X., Sun, Y., Wu, H., Xie, C., Chen, L., Liu, J., Wu, T., Jiang, S., Maureen, C., and Li, Z.: Characterizing the ratio of nitrate to sulfate in ambient fine particles of urban Beijing during 2018–2019, Atmos. Environ., 237, https://doi.org/10.1016/j.atmosenv.2020.117662, 2020.

Li, W., Sun, J., Xu, L., Shi, Z., Riemer, N., Sun, Y., Fu, P., Zhang, J., Lin, Y., Wang, X., Shao, L., Chen, J., Zhang, X., Wang, Z., and Wang W.: A conceptual framework for mixing

524   structures in individual aerosol particles, J. Geophys. Res.-Atmos., 121(22), 13784-

525   13798, https://doi.org/10.1002/2016JD025252, 2016.

526   Moffet, R., and Prather, K.: In-situ measurements of the mixing state and optical properties of

527   soot with implications for radiative forcing estimates, P. Natl. Acad. Sci. USA, 106(29),

528   11872-11877, https://doi.org/10.1073/pnas.0900040106, 2009.

529   Müller, A., Miyazaki, Y., Aggarwal, S., Kitamori, Y., Boreddy, S., and Kawamura, K.: Effects

530   of chemical composition and mixing state on size-resolved hygroscopicity and cloud

531   condensation nuclei activity of submicron aerosols at a suburban site in northern Japan

532   in   summer,   J.   Geophys.   Res.-Atmos.,   122(17),   9301-9318,

533   https://doi.org/10.1002/2017JD027286, 2017.

534   Peng, J. F., Hu, M., Guo, S., Du, Z. F., Zheng, J., Shang, D. J., Zamora, M., Zeng, L. M.,

535   Shao, M., Wu, Y. S., Zheng, J., Wang, Y., Glen, C., Collins, D., Molina, M., and Zhang,

536   R. Y.: Markedly enhanced absorption, and direct radiative forcing of black carbon under

537   polluted   urban   environments,   P.   Natl.   Acad.   Sci.   USA,   113,   4266–4271,

538   https://doi.org/10.1073/pnas.1602310113, 2016.

539   Petters, M. D. and Kreidenweis, S. M.: A single parameter representation of hygroscopic

540   growth and cloud condensation nucleus activity, Atmos. Chem. Phys., 7, 1961–1971,

541   https://doi.org/10.5194/acp-7-1961-2007, 2007.

542   Pierce, J. R., Chen, K., and Adams, P. J.: Contribution of primary carbonaceous aerosol to

543   cloud condensation nuclei: processes and uncertainties evaluated with a global aerosol

544   microphysics model, Atmos. Chem. Phys., 7, 5447–5466, https://doi.org/10.5194/acp-7-

545   5447-2007, 2007.

546   Pöschl, U., Letzel, T., Schauer, C., and Niessner, R.: Interaction of ozone and water vapor

547   with spark discharge soot aerosol particles coated with benzo[a]pyrene : O_3 and H_2O

548   adsorption, benzo[a]pyrene degradation, and atmospheric implications, J. Phys. Chem. A,

549   16, 105, https://doi.org/10.1021/jp004137n, 2001.

550   Ren, J., Zhang, F., Wang, Y., Collins, D., Fan, X., Jin, X., Xu, W., Sun, Y., Cribb, M., and Li,

551   Z.: Using different assumptions of aerosol mixing state and chemical composition to

552   predict CCN concentrations based on field measurements in urban Beijing, Atmos.

553   Chem. Phys., 18, 6907–6921, https://doi.org/10.5194/acp-18-6907-2018, 2018.

554   Ren, J., Zhang, F., Chen, L., Cao, G., Liu, M., Li, X., Wu, H., Cheng, Y., and Li, Z.:

555   Identifying the hygroscopic properties of fine aerosol particles from diverse sources in

556   urban atmosphere and the applicability in prediction of cloud nuclei, Atmos. Environ.,

557   298, 119615, https://doi.org/10.1016/j.atmosenv.2023.119615, 2023.

558   Riemer, N., Vogel, H., and Vogel, B.: Soot aging time scales in polluted regions during day

559   and night, Atmos. Chem. Phys., 4, 1885–1893, https://doi.org/10.5194/acp-4-1885-2004,

560   2004.

561   Riemer, N., Ault, A. P., West, M., Craig, R. L., and Curtis, J. H.: Aerosol mixing state:

562   Measurements, modeling, and impacts, Rev. Geophys., 57, 187–249,

563   https://doi.org/10.1029/2018RG000615, 2019.

564   Saha, P. K., Khlystov, A., and Grieshop, A. P.: Downwind evolution of the volatility and

565   mixing state of near-road aerosols near a US interstate highway, Atmos. Chem. Phys., 18,

566   2139–2154, https://doi.org/10.5194/acp-18-2139-2018, 2018.

567   Shi, J., Hong, J., Ma, N., Luo, Q., He, Y., Xu, H., Tan, H., Wang, Q., Tao, J., Zhou, Y., Han, S.,

568   Peng, L., Xie, L., Zhou, G., Xu, W., Sun, Y., Cheng, Y., and Su, H.: Measurement report:

569   On the difference in aerosol hygroscopicity between high and low relative humidity

570   conditions in the North China Plain, Atmos. Chem. Phys., 22, 4599–4613,

571   https://doi.org/10.5194/acp-22-4599-2022, 2022.

572   Spitieri, C., Gini, M., Gysel-Beer, M., and Eleftheriadis, K.: Annual cycle of hygroscopic

573   properties and mixing state of the suburban aerosol in Athens, Greece, Atmos. Chem.

574   Phys., 23, 235-249, https://doi.org/10.5194/acp-23-235-2023, 2023.

575   Stevens, R., and Dastoor, A.: A Review of the Representation of Aerosol Mixing State in

576   Atmospheric Models, Atmos., 10(4), 168, https://doi.org/10.3390/atmos10040168, 2019.

577   Sun, Y. L., Wang, Z. F., Du, W., Zhang, Q., Wang, Q. Q., Fu, P. Q., Pan, X. L., Li, J., Jayne, J.,

578   and Worsnop, D. R.: Longterm real-time measurements of aerosol particle composition

579   in Beijing, China: seasonal variations, meteorological effects, and source analysis,

580   Atmos. Chem. Phys., 15, 10149–10165, https://doi.org/10.5194/acp-15-10149-2015,

581   2015.

582   Swietlicki, E., Hansson, H. C., Hameri, K., Svenningsson, B., Massling, A., Mcfiggans, G., P.

583   Mcmurry, H., Petäjä, T., Tunved, P., Gysel, M., Topping, D., Weingartner, E.,

584   Baltensperger, U., Rissler, J., Wiedensohler, A., and Kulmala, M.: Hygroscopic

585   properties of submicrometer atmospheric aerosol particles measured with H-TDMA

586   instruments in various environments - a review, Tellus B, 60(3), 432–469,

587   https://doi.org/10.1111/j.1600-0889.2008.00350.x, 2008.

588   Wang, Y., Li, Z., Zhang, R., Jin, X., Xu, W., Fan, X., Wu, H., Zhang, F., Sun, Y., and Wang,

589   Q.: Distinct ultrafine- and accumulation-mode particle properties in clean and polluted

urban environments, Geophys. Res. Lett., 46, 10,918–10,925, https://doi.org/10.1029/2019GL084047, 2019.

Wang, Y., Ma, P.-L., Peng, J., Zhang, R., Jiang, J. H., Easter, R. C., and Yung, Y. L.: Constraining aging processes of black carbon in the Community Atmosphere Model using environmental chamber measurements, J. Adv. Model. Earth Sy., 10, 2514–2526. https://doi.org/10.1029/2018MS001387, 2018.

Wang, Z., Shi, C., Zhang, H., Chen, Y., Chi, X., Xia, C., Wang, S., Zhu, Y., Zhang, K., Chen, X., Xing, C., and Liu, C.: Measurement report: Dust and anthropogenic aerosols' vertical distributions over northern China dense aerosols gathered at the top of the mixing layer, Atmos. Chem. Phys., 23, 14271–14292, https://doi.org/10.5194/acp-23-14271-2023, 2023.

Winkler, P.: The growth of atmospheric aerosol particles as a function of the relative humidity—II. An improved concept of mixed nuclei, J. Aerosol Sci., 4(5), 373–387, https://doi.org/10.1016/0021-8502(73)90027-X, 1973.

Xie, C., He, Y., Lei, L., Zhou, W., Liu, J., Wang, Q., Xu, W., Qiu, Y., Zhao, J., Sun, J., Li, L., Li, M., Zhou, Z., Fu, P., Wang, Z., and Sun, Y.: Contrasting mixing state of black carbon-containing particles in summer and winter in Beijing, Environ. Pollut., 263, 114455, https://doi.org/10.1016/j.envpol.2020.114455, 2020.

Xu, W., Chen, C., Qiu, Y., Xie, C., Chen,Y., Ma, N., Xu, W., Fu, P., Wang, Z., and Pan, X.: Size-resolved characterization of organic aerosol in the North China Plain: new insights from high resolution spectral analysis, Environ. Sci.: Atmos., 1(6), 346–358, https://doi.org/10.1039/D1EA00025J, 2021.

Xu, W., Xie, C., Karnezi, E., Zhang, Q., Wang, J., Pandis, S. N., Ge, X., Zhang, J., An, J., Wang, Q., Zhao, J., Du, W., Qiu, Y., Zhou, W., He, Y., Li, Y., Li, J., Fu, P., Wang, Z., Worsnop, D. R., and Sun, Y.: Summertime aerosol volatility measurements in Beijing, China, Atmos. Chem. Phys., 19, 10205–10216, https://doi.org/10.5194/acp-19-10205-2019, 2019.

Yao, Y., Curtis, J. H., Ching, J., Zheng, Z., and Riemer, N.: Quantifying the effects of mixing state on aerosol optical properties, Atmos. Chem. Phys., 22, 9265–9282, https://doi.org/10.5194/acp-22-9265-2022, 2022.

Yu, F. and Luo, G.: Simulation of particle size distribution with a global aerosol model: contribution of nucleation to aerosol and CCN number concentrations, Atmos. Chem. Phys., 9, 7691–7710, https://doi.org/10.5194/acp-9-7691-2009, 2009.

Zhang, F., Wang, Y., Peng, J., Ren, J., Collins, D., Zhang, R., Sun, Y., Yang, X., and Li, Z.: Uncertainty in Predicting CCN Activity of Aged and Primary Aerosols, J. Geophys. Res.-Atmos., 122, 11723–11736, https://doi.org/10.1002/2017JD027058, 2017.

Zhang, J., Li, W., Wang, Y., Teng, X., Zhang, Y., Xu, L., Yuan, Q., Wu, G., Niu, H., and Shao, L.: Structural collapse and coating composition changes of soot particles during long-range transport, J. Geophys. Res.-Atmos., 128, e2023JD038871, https://doi.org/10.1029/2023JD038871, 2023.